Chaos, Solitons and Fractals 198 (2025) 116637

Contents lists available at ScienceDirect

Chaos, Solitons and Fractals

journal homepage: www.elsevier.com/locate/chaos

Chaos-induced hindrance of connectivity detection and topological unpredictability

Alessio Perinelli [a,b,*], Matteo Cescato [a], Roberto Iuppa [a,b], Leonardo Ricci [a,c]

[a] Department of Physics, University of Trento, Trento, 38123, Italy
[b] TIFPA-INFN, University of Trento, Trento, 38123, Italy
[c] CIMeC, Center for Mind/Brain Sciences, University of Trento, Rovereto, 38068, Italy

ARTICLE INFO

Keywords:
Networks
Connectivity
Correlation
Mutual information
Permutation entropy
Chaotic systems
Burridge–Knopoff model

ABSTRACT

The experimental assessment of networks within a complex system requires the inference of links. A common way to detect a link relies on the assumption that time series recorded out of two nodes contain sufficient shared information so as to detect a correlation, using either linear measures or more sensitive information-theoretical tools. While this assumption is theoretically granted for any system described by deterministically coupled differential equations, in an experimental scenario the emergence of chaotic regimes can hinder its validity. In this work we explore the issue of assessing connectivity in the prototypical case of a linear network of nonlinear oscillators, experimentally-implemented via a scalable electronic analog circuitry. Despite strong coupling, the assessed connectivity strength decays for an increasing length of the network. This phenomenon, which is interpreted in terms of a "topological unpredictability" of chaos, eventually leads to an apparent lack of connection between nodes that, in reality, are physically coupled. Our results provide insights on the difficulty of inferring links out of time series, with implications in the identification of networks in real systems, for example in Earth science and neuroscience.

1. Introduction

Given a complex system made of interacting subsystems, one of the most fundamental and challenging issues is the identification of collective behaviors: under certain conditions, a set of subsystems start showing correlations in the time evolution or, in other terms, a network of nodes connected by links appears [1]. The issue — shared by many fields ranging from economics [2] to social sciences [3] and engineering [4,5], and from Earth science [6–8] and climate research [9,10] to physiology [11] and neuroscience [12] — is ultimately tackled by solving two problems: identifying the existence and strength of a link between two nodes, and thereupon inferring a network structure in a set of mutually linked nodes [13].

From a mathematical perspective, a system made of interacting subsystems is described by a set of coupled differential equations. Absent a mathematical description, the existence and strength of a link are customarily determined by assessing correlation metrics out of time series of observables generated at each node. (Observables need not correspond to the same physical quantity.) Among the most used metrics [14,15], it is worth mentioning Pearson's cross-correlation and mutual information. While the former assumes a linear dependence between the two sources [2,16], it can be morphed into a nonlinear measure by introducing surrogate-based hypothesis testing [17]. Mutual information [18] is the prototypical information-theoretical measure that allows for the assessment of links according to the degree of information flowing between the nodes. Information-theoretical methods appear to be more powerful in terms of sensitivity and robustness to noise than their linear counterparts: quoting a seminal paper on the topic [19], "*in contrast to the linear correlation coefficient, [they are] sensitive also to dependences which do not manifest themselves in the covariance*". On the other hand, linear methods are more informative with regard to the significance of their outcomes, due to the availability of solid, theoretical estimates thereof [20].

A framework to describe collective behaviors is provided by the concept of synchronization, epitomized by the mutual frequency harmonization of two coupled linear oscillators, first observed by Huygens in pendulum clocks [21]. In the case of coupled, periodically oscillating subsystems, it is straightforward to define frequencies and phases, and thus to both theoretically and experimentally analyze synchronization. On the other hand, the scenario becomes far less clear in the case of chaotic oscillations, whose dynamics cannot be described in terms of a finite set of characteristic frequencies. While theoretical approaches

* Correspondence to: Department of Physics, University of Trento, Via Sommarive 14, 38123 Trento (TN), Italy.
E-mail address: alessio.perinelli@unitn.it (A. Perinelli).

https://doi.org/10.1016/j.chaos.2025.116637
Received 18 April 2025; Received in revised form 19 May 2025; Accepted 21 May 2025

based on a generalization of the definition of phases exist [22], the issue becomes challenging in experimental investigations, especially when the system at hand is a "black-box" accessible solely via recordings of scalar observables. Neglecting the trivial case of "complete" synchronization, whereby two coupled chaotic oscillators end up exhibiting exactly the same evolution [21], a crucial experimental question concerns to which extent correlation is detectable between networked systems in chaotic regimes. In other words, the question is whether — despite full determinism — coupled chaotic regimes can show such a diverse, "uncorrelated" dynamics that any possibility of detecting coupling out of time series is compromised.

These questions are pivotal in the investigation of time series recorded out of non-controllable systems, like brain and climate [23], in which the topological structure of the network is unknown. As a bridge between these natural, non-controllable systems and the theoretical world, experimental studies on small-scale networks of controllable nonlinear systems [24] allow for investigating in a more direct way the physics behind connectivity [25].

In this work we address the issues outlined above in a prototypical, controllable experimental system: a linear network of electronically-implemented Burridge–Knopoff (BK) oscillators [26,27]. In its original conception, a BK oscillator is the building element of a model of earthquake faults. Its electronic implementation is achievable by a relatively simple schematic relying on affordable electronic analog components [28]. The resulting reliability and versatility reflect in the reproducibility of the operation, the possibility of setting the dynamics by acting on a voltage parameter, as well as the simplicity of establishing arbitrary network topologies. With regard to the time evolution of systems made of at least two BK oscillators, robust chaotic regimes, as well as "spike-like" and "avalanche" behaviors reminiscent of neuron dynamics are promptly obtained [26,28]. Within a linear network consisting of up to 25 oscillators, we evaluate connectivity strength by means of two different estimators: Pearson's cross-correlation, and mutual information of the time series ordinal patterns (MIOP). This last measure combines the virtues of both mutual information and permutation entropy [29,30], resulting in a noise-robust and computationally-efficient tool to assess connectivity.

By evaluating connectivity for different lengths of the linear network, we show that — despite the system being fully deterministic and couplings between oscillators being "strong" — chaoticity hinders the capability of connectivity detection as the length increases, up to a point where correlation is completely washed out. This finding suggests that, besides the well-known temporal unpredictability of chaotic systems, quantified by the maximum Lyapunov exponent, a "topological unpredictability" exists. While temporal unpredictability implies that the evolution of a system beyond a certain temporal horizon is uncorrelated with the present state, topological unpredictability can be defined as the state of a subsystem being uncorrelated with the state of another subsystem beyond a certain topological horizon. Intriguingly, we find that the maximum correlation between oscillators decreases exponentially with the topological distance, in a striking analogy with exponential divergence of trajectories in the temporal domain.

The results of our study shed light on the issue of network identification in complex systems made of nonlinear, possibly chaotic oscillator units, providing a foothold for investigations on real cases addressing the dependence of the link strength on geometric and/or topological properties [31–34]. It might also be worth noting that, while previous works (see e.g. Ref. [35]) addressed the issue of how connectivity influences nonlinear dynamics, here the approach is the converse one, namely to investigate how nonlinear dynamics influences the detectability of connectivity.

The paper is organized as follows. The experimental implementation of the BK oscillator network is presented in Section 2. Correlation estimators are introduced in Section 3. Section 4 provides the results of the analysis and their interpretation in terms of topological unpredictability. Concluding remarks are drawn in Section 5.

2. Experimental setup and measurements

2.1. Network of BK oscillators

The BK model was first devised as a mechanical "spring-block" description of an earthquake fault [26]. Each massive block is coupled via springs to its nearest neighbors and connected, also via a spring, to an upper ceiling moving at constant speed; the horizontal surface on which the blocks lie exerts a nonlinear, velocity-dependent friction, in fact the only nonlinearity in the system. The system can be understood as a network of nonlinear stick–slip oscillators each being described by two state variables (position and speed). Consequently, if uncoupled from the others, a single oscillator can only produce a periodic motion [28]. Therefore, chaotic regimes in a network of BK oscillators can only emerge as a "collective" behavior, as opposed to more frequently investigated networks of systems that are autonomously capable of chaos [25]. In our model the oscillators are supposed to be "equal", modulo the slight differences provided by the intrinsic variability of the constituent devices and elements.

A natural gauge for the degree of coupling between BK oscillators is provided by the stiffness of the pulling spring connecting each block to the ceiling. So, a coupling can be deemed to be *strong* if the stiffness of the coupling springs is of the same order as the stiffness of the pulling springs, leading to the coupling terms in the differential equations to be of the same order of the autonomous terms. The coupling is then *diffusive*, as it depends on the difference between the oscillators' states, and *linear*, since this dependence is described by Hooke's law [21].

A more handily strategy to experimentally address the dynamics of the BK model is to implement an electronic analog. Indeed, mimicking dynamical systems by means of electronic analog circuits is a powerful approach to simulate and investigate complex systems, like lasers [36] and neurons [24], complementary to a merely computational approach. A first crucial aspect to highlight is the intrinsic variability of the electronic components, which results in the absence of the artificial symmetry within the system that one faces in numerical simulations. The experimental platform used in the present work consists of a board hosting 25 BK oscillators, whose electronic implementation and governing equations are detailed in Ref. [28]. The platform is indeed a scaled-up version of the pair of oscillators discussed there, and it consists of a single printed circuit with a common power supply. The dynamics of a BK oscillator is described by two state variables, a "pseudo-position" W and a "pseudo-speed" V, both mapped as voltages. The only parameter that controls the dynamics is the "pseudo-speed" of the driving ceiling, also mapped through a voltage V_d.

A second crucial aspect is the fact that the physical delays due to signal propagation within the circuit, whose size is of order $30\,\mathrm{cm}$, are of order $1\,\mathrm{ns}$, which is negligible as compared with the single oscillator's period, of order $1\,\mathrm{ms}$, as well as with the reciprocal of the op-amp bandwidth, of order $1\,\mu\mathrm{s}$. Consequently, the coupling is *de facto* instantaneous and thus oscillators can be regarded as being at a vanishing physical distance from one another. The coupling induces a *topological* structure in the system, rather than a spatial one. In this sense, the distance between the end oscillators of an M-fold chain, equal to the number $M-1$ of physical links, is to be intended as a topological distance rather than a physical one.

2.2. Setup and measurements

The circuit board, hosting 25 BK oscillators, is powered by a bench power supply with $\pm 12\,\mathrm{V}$ and drawing about $5\,\mathrm{W}$. In principle, each BK oscillator can be connected with any four other ones, thus allowing for a wide range of network topologies. In the present study, we connected M oscillators in a linear chain, where M is an integer varying from 2 to 25. Given an M-fold chain, we henceforth label the ith BK oscillator as B_i, with $1 \leqslant i \leqslant M$. Consequently, B_1 and B_M are connected to B_2

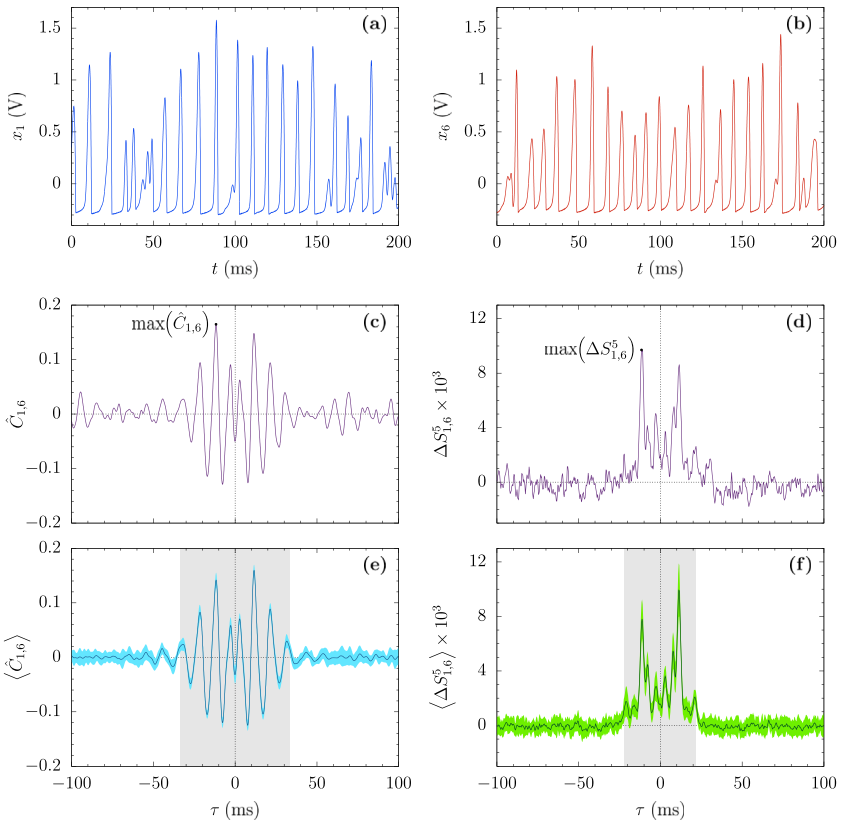

Fig. 1. Example of evaluation of the cross-correlation and the 5th-order MIOP between the end oscillators $\mathcal{B}_1$, $\mathcal{B}_6$ of a 6-fold chain of BK oscillators. **(a)** "Pseudo-speed" voltage signal x_1 sampled from the oscillator $\mathcal{B}_1$ as a function of t. **(b)** Signal x_6 sampled from the oscillator $\mathcal{B}_6$. **(c)** Cross-correlation $\hat{C}_{1,6}$, as a function of the lag τ, evaluated on a single pair of 10^6-point segments of the time series simultaneously collected from the oscillators $\mathcal{B}_1$ and $\mathcal{B}_6$ (see main text). The maximum value $\max\left(\hat{C}_{1,6}\right)$ of $\hat{C}_{1,6}$ is highlighted. **(d)** 5th-order incremental MIOP $\Delta S^5_{1,6}$ computed on the same segments considered in (c). **(e)** Average cross-correlation $\left\langle \hat{C}_{1,6} \right\rangle$ computed out of 16 independent pairs of 10^6-point segments. The light-blue shaded area represents the related uncertainty. The gray shaded area corresponds to the narrowest lag range being symmetric about the origin and such that, outside it, the average cross-correlation differs from zero by less than twice its uncertainty. **(f)** As in (e) but for the average 5th-order incremental MIOP $\left\langle \Delta S^5_{1,6} \right\rangle$. (For interpretation of the references to color in this figure legend, the reader is referred to the web version of this article.)

and $\mathcal{B}_{M-1}$, respectively, while $\mathcal{B}_i$, with $2 \leqslant i \leqslant M-1$, is connected to both $\mathcal{B}_{i\pm1}$.

The oscillators share the same control voltage V_d. This control parameter is provided by an external control-and-acquisition board based on a system-on-chip (Xilinx Zynq-Z7010) running a custom firmware and connected to a workstation via Ethernet. The system-on-chip, which combines a field-programmable gate array (FPGA) with a general purpose processor, drives simultaneously 8 analog-to-digital converters (ADCs), each working with 12-bit resolution at a sampling frequency of 1 MHz. Real-time averaging of 16 consecutive samples results, for each one of the 8 channels, in an improved resolution of 16 bit and an effective sampling frequency of 62.5 kHz, corresponding to a sampling period $T = 16\,\mu\mathrm{s}$. The sampling frequency largely overcomes the spectrum shown by the network dynamics ($\lesssim 5$ kHz). The implemented control-and-acquisition setup allows for automatizing the data acquisition process in a versatile, reproducible, and reliable manner, which is typical of FPGA-based solutions [37].

In a typical acquisition, the "pseudo-speed" signal generated by an oscillator is sampled over a time span of 500 s, thus producing a sequence of 31 250 001 points. Each time series is then partitioned into 31 consecutive, non-overlapping segments of $N \cong 10^6$ points. In order to obtain a collection of independent time series, the even-numbered segments — the 2nd, the 4th, …, the 30th — are discarded. As a result, for each sampled time series, 16 segments, each spanning about 16 s and separated by at least the same time, are available.

Let $x_i(t)$ be the "pseudo-speed" voltage signal of the ith oscillator $\mathcal{B}_i$, with $1 \leqslant i \leqslant M$, and let $x_i[n] = x_i(nT)$ be the corresponding sampled sequence, with $0 \leqslant n \leqslant N-1$, $n \in \mathbb{Z}$. Given the sequence $x_i[n]$, let $\hat{\mu}_i$, $\hat{\sigma}_i^2$ be the related sample mean and sample variance, respectively. Examples of the time series recorded for two BK oscillators are shown in Fig. 1(a),(b).

3. Connectivity estimators

3.1. Cross-correlation

The cross-correlation $C_{i,j}(\tau)$ between $\mathcal{B}_i$ and $\mathcal{B}_j$ is defined as a function of the lag τ as follows:

$$C_{i,j}(\tau) = \frac{\left\langle \left[x_i(t) - \mu_i\right]\left[x_j(t+\tau) - \mu_j\right] \right\rangle}{\sigma_i \sigma_j},$$

where the operator $\langle\cdot\rangle$ indicates the ensemble average, while μ_k, σ_k, with $k = i, j$, are the population mean and the population standard deviation of $x_k(t)$, respectively. An estimator of the cross-correlation in the case of a lag $\tau = \ell T$, $\ell \in \mathbb{Z}$, is given by

$$\hat{C}_{i,j}(\ell T) = \frac{\hat{c}_{i,j}(\ell T) - \hat{\mu}_i \hat{\mu}_j}{\hat{\sigma}_i \hat{\sigma}_j},$$

where

$$\hat{c}_{i,j}(\ell T) = \sum_{k=\max(0,-\ell)}^{N-1-\max(0,\ell)} \frac{x_i[k]\, x_j[k+\ell]}{N - |\ell|}.$$

A lag-independent estimate of the error on a single evaluation of $\hat{C}_{i,j}(\ell T)$ can be obtained by error propagation, provided that $N \gg |\ell|$

and assuming homoskedasticity concerning the uncertainty of the single voltage samples. So we have

$$\hat{\sigma}_{\hat{C}_{i,j}} \approx \frac{\sqrt{\hat{\sigma}_i^2 + \hat{\sigma}_j^2 + 2\left(\hat{\mu}_i^2 + \hat{\mu}_j^2\right)}}{\hat{\sigma}_i \hat{\sigma}_j} \frac{\sigma_x}{\sqrt{N}} ,$$

where σ_x is the common uncertainty on the single voltage samples, which was found to be about 0.3 mV.

To measure the connectivity strength between $\mathcal{B}_i$ and $\mathcal{B}_j$, we consider the maximum value $\max\left(\hat{C}_{i,j}\right)$ of $\hat{C}_{i,j}(\ell T)$,

$$\max\left(\hat{C}_{i,j}\right) = \max_{\forall \ell} \left[\hat{C}_{i,j}(\ell T)\right] ,$$

computed on two segments recorded simultaneously. The procedure is repeated for all 16 segment pairs. The final value of connectivity strength is then taken as the sample mean of the resulting 16 maximum values, with the sample standard deviation providing the related uncertainty.

An example of the evaluation of the cross-correlation between the time series recorded for two BK oscillators is shown in Fig. 1(c),(e).

3.2. Mutual information of time series ordinal patterns

MIOP is a measure of the amount of information shared by two scalar time series. It relies on symbolic encoding, as follows. Given the sequence $x_i[n]$ sampled from the oscillator $\mathcal{B}_i$ and an integer dimension $m \geqslant 2$, we consider, for any n such that $0 \leqslant n \leqslant N - m$, the m-tuple, or trajectory,

$$\mathbf{x}_{i,n} = \left(x_i[n],\, x_i[n+1],\, \ldots,\, x_i[n+m-1]\right) .$$

The trajectory is then encoded into the symbolic sequence, henceforth referred to as a word,

$$\mathbf{s}_{i,n}^m = \left(s_{i,n}^0,\, s_{i,n}^1,\, \ldots,\, s_{i,n}^{m-1}\right) ,$$

where the integer $s_{i,n}^k$, with $k = 0, 1, \ldots, m-1$, corresponds to the rank of $x_i[n+k]$ within $\mathbf{x}_{i,n}$, namely, the position, denoted by an integer in the range $[0, m-1]$, that $x_i[n+k]$ would have within the same m-tuple sorted in ascending order. In the case of an equality between two or more elements of $\mathbf{x}_{i,n}$, the relative rank is provided by the index k. The number of possible words of order m is given by the number of permutations of $0, 1, \ldots, m-1$, namely $m!$. As a straightforward generalization, we can state that the sequence $x_i[n]$ is encoded into a sequence $\left\{\mathbf{s}_{i,n}^m\right\}$ of words of order m, with $0 \leqslant n \leqslant N - m$.

Besides $x_i[n]$, we now consider also the sequence $x_j[n]$ stemming from the oscillator $\mathcal{B}_j$ as well as its encoded sequence $\left\{\mathbf{s}_{j,n}^m\right\}$. The two sequences of words are then merged, with a variable lag $\tau = \ell T$, $\ell \in \mathbb{Z}$, to obtain the joint sequence

$$\left\{\left(\mathbf{s}_{i,n},\, \mathbf{s}_{j,n+\ell}\right)\right\} ,$$

with $n = \max(0, -\ell), \ldots, N - 1 - \max(0, \ell)$, and where each pairing $\left(\mathbf{s}_{i,n},\, \mathbf{s}_{j,n+\ell}\right)$ can be interpreted as a "vector concatenation".

Given a lag ℓT, the occurrences of each of the $(m!)^2$ possible joint words, denoted by $S_{k',k''}$ (with $k',\, k'' = 1, 2, \ldots, m!$), are counted in order to obtain the corresponding lag-dependent joint relative frequency $\hat{p}_{i,j}^{\ell}\left(S_{k',k''}\right)$. The mth-order MIOP $S_{i,j}^m(\ell T)$ between $\mathcal{B}_i$ and $\mathcal{B}_j$ is finally evaluated as

$$S_{i,j}^m(\ell T) = \sum_{k'=1}^{m!} \sum_{k''=1}^{m!} \hat{p}_{i,j}^{\ell}\left(S_{k',k''}\right) \ln\left[\frac{\hat{p}_{i,j}^{\ell}\left(S_{k',k''}\right)}{\hat{p}_i^{\ell}(k')\, \hat{p}_j^{\ell}(k'')}\right] ,$$

where

$$\hat{p}_i^{\ell}(k') = \sum_{k''=1}^{m!} \hat{p}_{i,j}^{\ell}\left(S_{k',k''}\right) ,$$

$$\hat{p}_j^{\ell}(k'') = \sum_{k'=1}^{m!} \hat{p}_{i,j}^{\ell}\left(S_{k',k''}\right)$$

are the marginal relative frequencies. In the expression of $S_{i,j}^m(\ell T)$, we use the natural logarithm.

In the present work, MIOP is evaluated for $m = 5$ and, as a trade-off to avoid redundance and irrelevance, upon downsampling each time series by a factor of 20, thus reducing the number of points $N = 10^6$ to $5 \cdot 10^4$.

In the case of pairs of non-adjacent BK oscillators, for large absolute values of the lag τ, $|\tau| \gtrsim 0.3$ s, the 5th-order MIOP $S_{i,j}^5(\tau)$ tends to fluctuate about a constant value $\bar{S}_{i,j}^5$. Therefore, also for the sake of comparison, rather than MIOP we consider henceforth the incremental MIOP $\Delta S_{i,j}^5(\tau)$, defined as

$$\Delta S_{i,j}^5(\tau) = S_{i,j}^5(\tau) - \bar{S}_{i,j}^5 .$$

In this last expression, the baseline $\bar{S}_{i,j}^5$ is obtained by averaging $S_{i,j}^5(\tau)$ on the lag values $288\,\text{ms} < |\tau| \leqslant 320\,\text{ms}$.

Conversely, in the case of adjacent oscillators, i.e. when $j = i \pm 1$, the baseline $\bar{S}_{i,j}^5$ is more difficult to evaluate, as MIOP decays too slowly with $|\tau|$. For this reason we use as a reference $\bar{S}_{i,j}^5$ the baseline inferred by considering pairs of independent time series sampled at different times from a single "reference" oscillator, as described in Section 4.2.

As for cross-correlation, the maximum value of $\Delta S_{i,j}^5(\tau)$ can be considered as a measure of the connectivity strength between $\mathcal{B}_i$ and $\mathcal{B}_j$. Also in this case, for each pair of coupled oscillators considered, the search for the maximum incremental MIOP $\max\left(\Delta S_{i,j}^5\right)$ is repeated for each independent pair of time series collected from the two oscillators, summarizing the results with their sample mean and their sample standard deviation.

An example of the evaluation of the 5th-order incremental MIOP between the time series recorded for two BK oscillators is shown in Fig. 1(d),(f).

4. Dependence of connectivity on topological distance

In this Section, we finally discuss the measurements and the analysis of the dependence of connectivity on topological distance.

Henceforth, given an $(M+1)$-fold chain of BK oscillators, we consider the "pseudo-speed" signals simultaneously sampled from the end oscillators $\mathcal{B}_1$, $\mathcal{B}_{M+1}$. The two oscillators turn out to be separated by a topological distance M. For the sake of clarity, with regard to the connectivity estimators introduced in Section 3, we define the cross-correlation $\hat{C}_M(\tau)$ and the 5th-order incremental MIOP $\Delta S_M^5(\tau)$ as

$$\hat{C}_M(\tau) \equiv \hat{C}_{1,M+1}(\tau) ,$$
$$\Delta S_M^5(\tau) \equiv \Delta S_{1,M+1}^5(\tau) ,$$

respectively. The maximum values $\max\left(\hat{C}_M\right)$, $\max\left(\Delta S_M^5\right)$ are defined accordingly.

4.1. Periodic behavior

For appropriate values of the control voltage V_d, the BK oscillators exhibit a periodic behavior. As an example, Fig. 2 shows the Lissajous curves of the end oscillators of a 10-fold chain ($M = 9$) in two different regimes. The plot in Fig. 2(a) reveals a periodic behavior, which is apparent from the regular shape of the curve. In this case, the connectivity estimators $\max\left(\hat{C}_M\right)$ and $\max\left(S_M^5\right)$ amount to about 0.7 and 1.1, respectively. Compared with the results obtained in the chaotic regime (Fig. 2(b)) and discussed below, the reported values reveal the presence of a significant correlation between the two end oscillators.

It is worth noticing that for all other measurements reported in the present work the control voltage V_d is set to 0 V to ensure chaotic behavior.

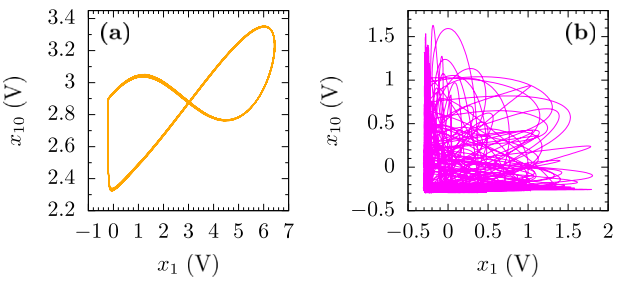

Fig. 2. Lissajous curves of the "pseudo-speed" voltage signals x_1, x_{10} sampled from the end oscillators $\mathcal{B}_1$, $\mathcal{B}_{10}$ of a 10-fold chain of BK oscillators ($M = 9$): **(a)** periodic regime, obtained with $V_d = 2.8\,\mathrm{V}$; **(b)** chaotic regime, obtained with $V_d = 0\,\mathrm{V}$.

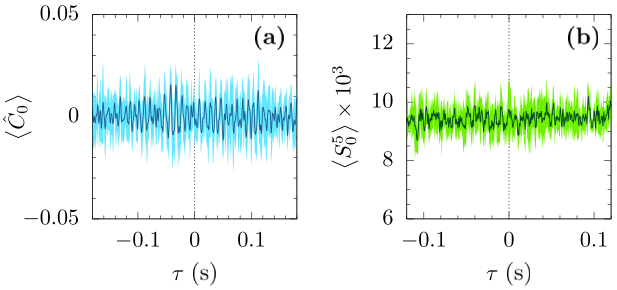

Fig. 3. **(a)** Average cross-correlation $\langle \hat{C}_0 \rangle$ and **(b)** average 5th-order MIOP $\langle S_0^5 \rangle$, both as a function of the lag τ, computed from 8 pairs of independent 10^6-point time series sampled from the same BK oscillator (end oscillator $\mathcal{B}_0$ in a 25-fold chain) at different times. In both plots, the shaded area represents the uncertainty of the related connectivity estimator.

4.2. Assessment of the connectivity estimator baselines

Fig. 3 shows the cross-correlation and the 5th-order MIOP computed from 8 pairs of independent time series sampled from the same oscillator at different times. These pairs are obtained by pairing two sets of 8 segments resulting from the segmentation of an experimental time series as described in Section 2.2.

As highlighted in Fig. 3, the cross-correlation fluctuates by construction about zero. Conversely, MIOP fluctuates about a constant value $\bar{S}_0^5$. This very level is taken as a reference for MIOP assessments in the case of adjacent oscillators, as anticipated in Section 3.2. It is worth noting that this reference baseline is compatible with the baselines that are inferred from MIOP values computed at large lag ($|\tau| \gtrsim 0.3\,\mathrm{s}$) for each $(M+1)$-fold chain, with $M \geqslant 2$.

4.3. Chaotic behavior and predictability horizon in the topological domain

Figs. 4 and 5 show the cross-correlation $\hat{C}_M(\tau)$ and the incremental MIOP $\Delta S_M^5(\tau)$, respectively, for $1 \leqslant M \leqslant 24$.

It is worth noting that, in a periodic regime, noise is present, which, however, does not hinder the emergence of a correlated behavior. On the other hand, in a chaotic regime and despite being driven by the very same set of coupled differential equations, the system does not produce anymore a correlated behavior: correlation between oscillators vanishes, regardless of the delay, provided that the length of the chain is sufficiently large.

The maximum values taken on by cross-correlation and MIOP as a function of the chain length M are shown in Fig. 6. As qualitatively shown in Figs. 4, 5, these maxima decrease with M. Interestingly, this decrease appears to be exponential with M for both metrics, up to $M \gtrsim 9$. Beyond this point, the values settle to a minimum given by the noisy fluctuations of cross-correlation and MIOP in the case of uncorrelated sources.

A linear fit to $\ln\left[\max\left(\hat{C}_M\right)\right]$ as a function of M in the interval $3 \leqslant M \leqslant 8$, which corresponds to an exponential decay of $\max\left(\hat{C}_M\right)$ as $\exp(-M/M_C)$, yields $M_C = 2.6 \pm 0.2$. The very same procedure applied to $\ln\left[\max\left(\Delta S_M^5\right)\right]$ yields a decay constant equal to $M_S = 2.0 \pm 0.2$. Remarkably, the decay constants M_C, M_S are compatible, suggesting that the rate of correlation loss is independent of the metric used for its assessment.

This observation suggests that, analogously to the time-domain predictability horizon induced by a positive Lyapunov exponent, there exists a *topological* predictability horizon induced by chaos and by the topology of couplings, and quantified by the decay constants M_C, M_S.

5. Discussion

Leveraging on an experimental nonlinear electronic system, we provided evidence that for a network in a chaotic regime the dynamics of constituent units — despite being fully deterministic and instantaneously coupled — wind up being uncorrelated. This observation holds for two connectivity metrics, completely unrelated from one another — linear cross-correlation and nonlinear information-theoretical MIOP metric — thus hinting at an universal phenomenon. More in detail, we showed that the effect of chaos on a topologically structured set of subsystems (in this case, a linear chain) turns out to be an exponential reduction in connectivity strength as the topological distance increases. This exponential reduction can be interpreted in terms of a topological unpredictability of the system, which parallels the temporal unpredictability of chaos. The result has crucial implications in the identification of networks in real systems: the observed topological unpredictability poses, in chaotic regimes, an upper limit to the degree of correlation that two nodes can express.

One might argue that topological unpredictability arises as a by-product of the combination of Lyapunov exponents and the time typically required to a signal to propagate through a chain. However, for $M \geqslant 3$, the time-dependent correlation patterns displayed in Figs. 4, 5 do not show any significant relationship between time lag τ and M, and thus between τ and the physical distance. Consequently, correlations indeed appear as collective phenomena that make the argument of signal propagation a non-starter.

Besides being an interesting concept to be further explored from the point of view of chaos theory, the observation of topological unpredictability prompts some intriguing speculations concerning complex systems in nature. For example, one might model — in an oversimplistic way — the Earth climate as a very large system made of smaller units, e.g. convection cells, that are driven by a deterministic dynamics and are coupled with each other in a nearest-neighbor fashion. The whole system would be described by a large set of N coupled differential equations. Nonetheless, according to the results of the present work, the chaotic nature of the dynamics would induce a topological — and, in this example, also spatial — unpredictability.

Going back to the inceptive geophysical problem from which the BK model was devised, one might propose a similar consideration regarding an earthquake fault modeled as a set of N coupled BK oscillators. In a chaotic regime, the evolution of a given part of the fault is not expected to provide any information on the evolution of another part, *even if the dynamics were fully deterministic*. A further major example could concern neuronal networks, which are prominent examples of topologically-structured nonlinear oscillators. In this case, the topological unpredictability ensuing from a chaotic regime would allow for higher activity variability — and thus information processing capability — within the network [35]. In this context, and as a first possible development of the present work, given the spike-like nature of the dynamics of BK oscillators, it might prove fruitful to address connectivity also by relying on point-process techniques [38,39].

It is worth highlighting that, in the present work, symmetrically, instantaneously and bidirectionally coupled systems were considered. On the one hand, we avoided introducing delays, which in fact play a

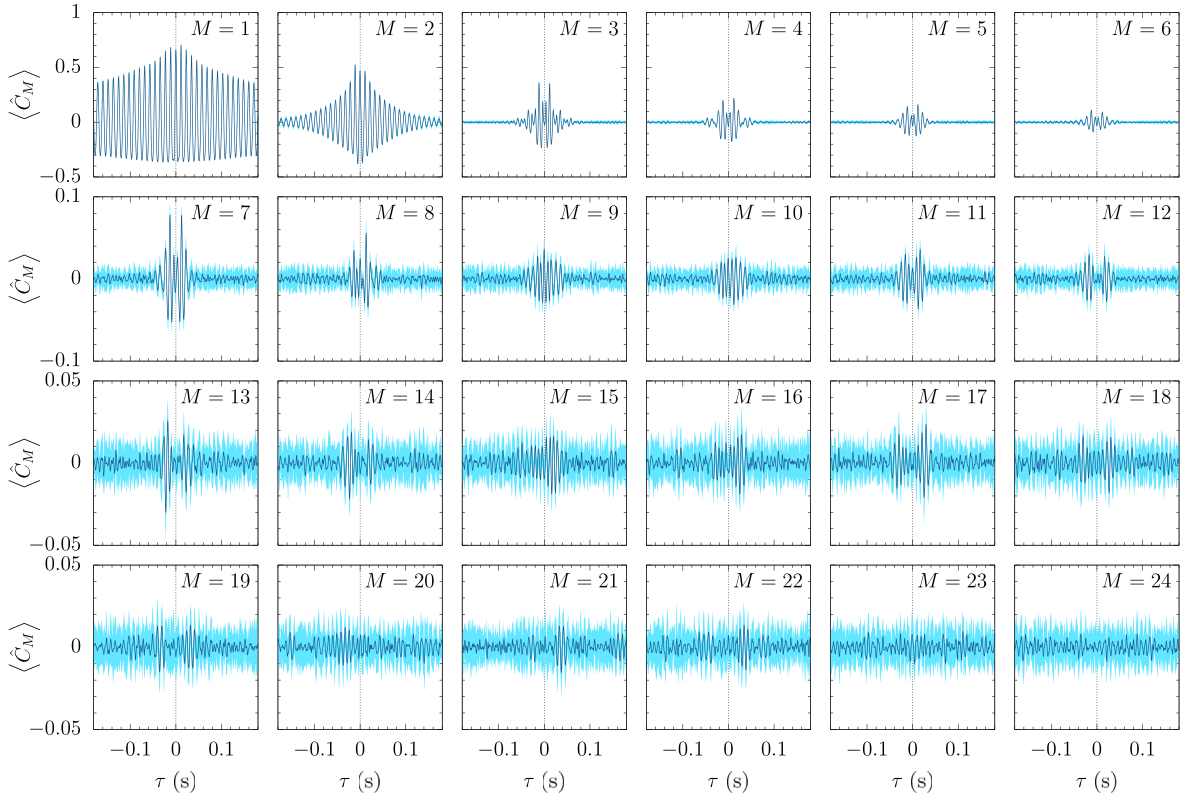

Fig. 4. Average cross-correlation $\langle \hat{C}_M \rangle$, as a function of the lag τ, between the end oscillators B_1, B_{M+1} of $(M+1)$-fold chains, with $1 \leqslant M \leqslant 24$. For each value of the distance M, the cross-correlation is estimated by averaging the cross-correlation values obtained from 16 independent pairs of 10^6-point time series (see Section 3.1). The light-blue shaded area represents the uncertainty. (For interpretation of the references to color in this figure legend, the reader is referred to the web version of this article.)

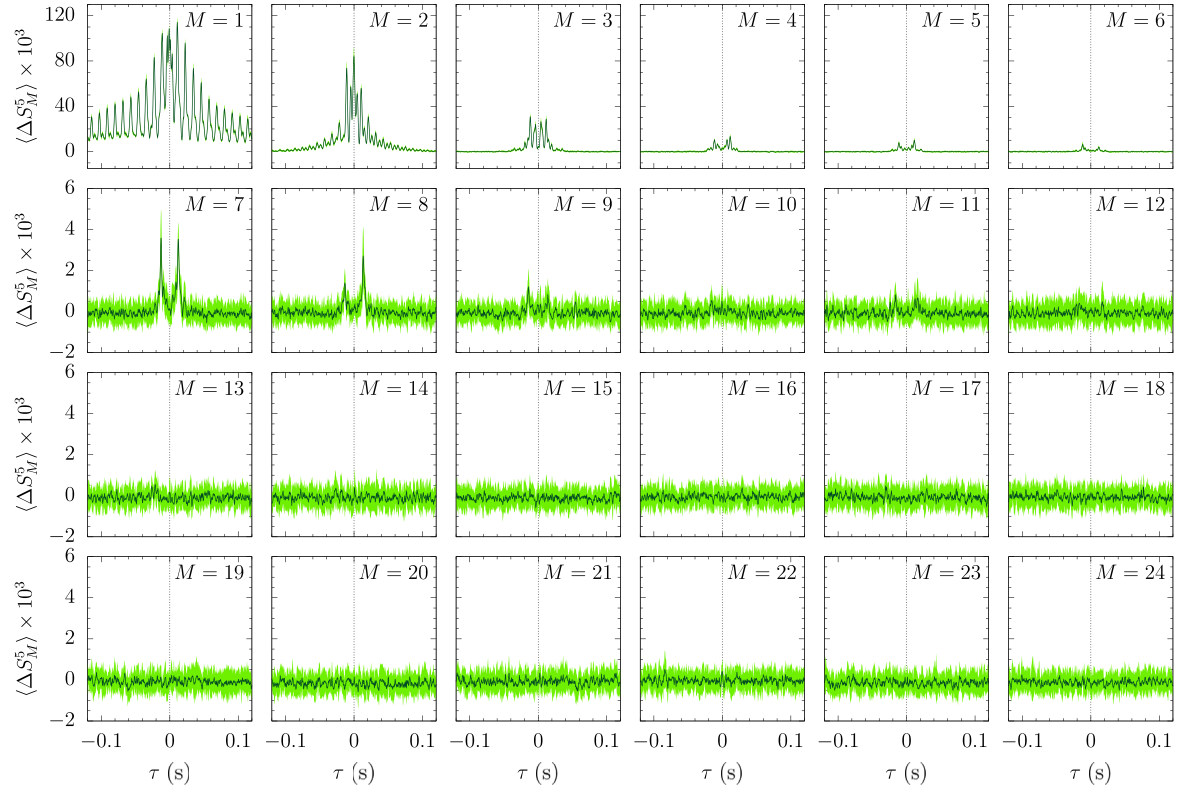

Fig. 5. Average 5th-order incremental MIOP $\langle \Delta S_M^5 \rangle$, as a function of the lag τ, between the end oscillators B_1, B_{M+1} of $(M+1)$-fold chains, with $1 \leqslant M \leqslant 24$. For each value of the distance M, MIOP is estimated by averaging MIOP values obtained from 16 independent pairs of 10^6-point time series (see Section 3.2). The light-green shaded area represents the uncertainty. (For interpretation of the references to color in this figure legend, the reader is referred to the web version of this article.)

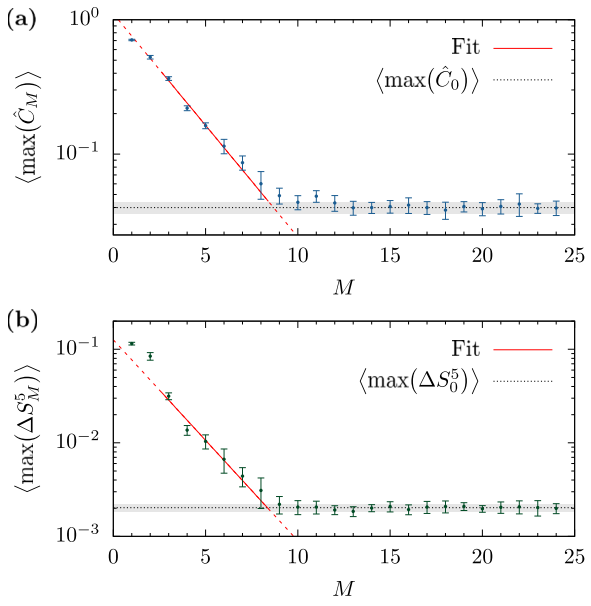

Fig. 6. **(a)** Average maximum cross-correlation $\langle \max(\hat{C}_M) \rangle$ and **(b)** average maximum 5th-order incremental MIOP $\langle \max(\Delta S_M^5) \rangle$ between the end oscillators $\mathcal{B}_1$, $\mathcal{B}_{M+1}$ of $(M+1)$-fold chains, both as a function of the distance M separating $\mathcal{B}_1$ and $\mathcal{B}_{M+1}$. Each experimental point corresponds to the sample average of 16 independent calculations (see Section 3). The error bars represent the corresponding sample standard deviations. The dashed black lines represent the values of $\langle \max(\hat{C}_M) \rangle$ and $\langle \max(\Delta S_M^5) \rangle$ computed out of independent time series collected from the same oscillator (end oscillator $\mathcal{B}_0$ in a 25-fold chain) at different times (see Section 4.2); the gray shaded areas indicate the related uncertainties. For both log-scale plots, a straight line (red) is fitted to the experimental points obtained for $3 \leqslant M \leqslant 8$. (For interpretation of the references to color in this figure legend, the reader is referred to the web version of this article.)

significant role in the real systems mentioned above. On the other hand, we overlooked the issue of directionality, namely whether there are differences in the way node 1 influences/forecasts node 2 with respect to the way node 2 influences node 1. The issue of link directionality was first tackled by Granger [40], who introduced the "causality" measure named after him for bivariate linear models. The concept was then widened to address multivariate linear models [41,42] and nonlinear systems [43,44]. Also in this case, for reasons similar to the ones mentioned above, information-theoretical methods [45–48] have become more attractive than their linear or nonlinear parametric counterparts due to their being model-free and less noise-vulnerable. Future developments of the present work include the extension of the investigation to address directionality by exploiting the versatility of the available experimental setup. To the purpose of addressing directionality, an additional possible research direction consists of exciting the BK oscillators and to observe the network's response [49].

Although the approach followed in the present work is to investigate connectivity in a linear chain by analyzing the correlation of the two end oscillators, an important future step would be to carry out the analysis considering all possible pairs. In principle, this more complex analysis should provide comparable results with respect to the present assessment of topological unpredictability. Nevertheless, a possible variability of the decay constants M_C, M_S along the chain might emerge as a consequence of the intrinsic variability of the circuit parameters.

Possibly the most relevant development of the present study would concern configurations beyond the simple chain topology discussed above. As a first step, one could consider two-dimensional configur ations — i.e. lattices of BK oscillators — that can be easily assembled by means of the experimental platform used here, or any extension thereof. These configurations could present different local and nonlocal topological properties and different degrees of symmetry, for example ordered lattices or hub-leaves structures. Addressing two-dimensional configurations is expected to provide elements to better understand the origin of topological unpredictability and the role of the network diameter.

Finally, while the present MIOP analysis was carried out for a single value of the dimension $m = 5$, it would be worth investigating MIOP for different values of m.

CRediT authorship contribution statement

Alessio Perinelli: Writing – original draft, Methodology, Formal analysis. **Matteo Cescato:** Writing – original draft, Software, Data curation. **Roberto Iuppa:** Writing – review & editing, Visualization, Funding acquisition. **Leonardo Ricci:** Writing – original draft, Methodology, Formal analysis.

Declaration of competing interest

The authors declare the following financial interests/personal relationships which may be considered as potential competing interests: Two authors, Alessio Perinelli and Leonardo Ricci, are serving as Associate Editors for Chaos, Solitons, & Fractals.

Acknowledgments

The authors thank the Italian Space Agency for the financial support under the contract ASI "LIMADOU Scienza+" n. 2020-31-HH.0.

Data availability

Data will be made available on request.

References

[1] Albert R, Barabási A-L. Statistical mechanics of complex networks. Rev Modern Phys 2002;74:47–97. http://dx.doi.org/10.1103/RevModPhys.74.47.
[2] Mantegna RN. Hierarchical structure in financial markets. Eur Phys J B 1999;11(1):193–7. http://dx.doi.org/10.1007/s100510050929.
[3] Borgatti SP, Mehra A, Brass DJ, Labianca G. Network analysis in the social sciences. Science 2009;323:892–5. http://dx.doi.org/10.1126/science.1165821.
[4] Filatrella G, Nielsen AH, Pedersen NF. Analysis of a power grid using a kuramoto-like model. Eur Phys J B 2008;61:485–91. http://dx.doi.org/10.1140/epjb/e2008-00098-8.
[5] Pagani GA, Aiello M. The power grid as a complex network: A survey. Phys A 2013;392:2688–700. http://dx.doi.org/10.1016/j.physa.2013.01.023.
[6] Abe S, Suzuki N. Scale-free network of earthquakes. Europhys Lett 2004;65:581. http://dx.doi.org/10.1209/epl/i2003-10108-1.
[7] Abe S, Suzuki N. Complex earthquake networks: Hierarchical organization and assortative mixing. Phys Rev E 2006;74:026113. http://dx.doi.org/10.1103/PhysRevE.74.026113.
[8] Baiesi M, Paczuski M. Scale-free networks of earthquakes and aftershocks. Phys Rev E 2004;69:066106. http://dx.doi.org/10.1103/PhysRevE.69.066106.
[9] Tsonis AA, Swanson KL, Roebber PJ. What do networks have to do with climate? Bull Am Meteorol Soc 2006;87(5):585–95. http://dx.doi.org/10.1175/BAMS-87-5-585.
[10] Gelbrecht M, Boers N, Kurths J. A complex network representation of wind flows. Chaos 2017;27(3):035808. http://dx.doi.org/10.1063/1.4977699.
[11] Bartsch RP, Liu KK, Bashan A, Ivanov PC. Network physiology: How organ systems dynamically interact. PLoS One 2015;10:e0142143. http://dx.doi.org/10.1371/journal.pone.0142143.
[12] Buckner RL, Andrews-Hanna JR, Schacter DL. The brain's default network. Ann New York Acad Sci 2008;1124(1):1–38. http://dx.doi.org/10.1196/annals.1440.011.
[13] Yu D, Parlitz U. Inferring network connectivity by delayed feedback control. PLoS One 2011;6:1–12. http://dx.doi.org/10.1371/journal.pone.0024333.
[14] Rubido N, Martí AC, Bianco-Martínez E, Grebogi C, Baptista MS, Masoller C. Exact detection of direct links in networks of interacting dynamical units. New J Phys 2014;16:093010. http://dx.doi.org/10.1088/1367-2630/16/9/093010.
[15] Rossini PM, Di Iorio R, Bentivoglio M, Bertini G, Ferreri F, Gerloff C, et al. Methods for analysis of brain connectivity: An IFCN-sponsored review. Clin Neurophysiol 2019;130:1833–58. http://dx.doi.org/10.1016/j.clinph.2019.06.006.

[16] de Pasquale F, Della Penna S, Snyder AZ, Lewis C, Mantini D, Marzetti L, et al. Temporal dynamics of spontaneous MEG activity in brain networks. Proc Natl Acad Sci 2010;107(13):6040–5. http://dx.doi.org/10.1073/pnas.0913863107.
[17] Perinelli A, Chiari DE, Ricci L. Correlation in brain networks at different time scale resolution. Chaos: Interdiscip J Nonlinear Sci 2018;28:063127. http://dx.doi.org/10.1063/1.5025242.
[18] Schreiber T. Measuring information transfer. Phys Rev Lett 2000;85:461–4. http://dx.doi.org/10.1103/PhysRevLett.85.461.
[19] Kraskov A, Stögbauer H, Grassberger P. Estimating mutual information. Phys Rev E 2004;69:066138. http://dx.doi.org/10.1103/PhysRevE.69.066138.
[20] Perinelli A, Castelluzzo M, Tabarelli D, Mazza V, Ricci L. Relationship between mutual information and cross-correlation time scale of observability as measures of connectivity strength. Chaos 2021;31:073106. http://dx.doi.org/10.1063/5.0053857.
[21] Pikovsky A, Rosenblum M, Kurths J. Synchronization. A universal concept in nonlinear science. Cambridge University Press; 2001.
[22] Rosenblum MG, Pikovsky AS, Kurths J. Phase synchronization of chaotic oscillators. Phys Rev Lett 1996;76:1804–7. http://dx.doi.org/10.1103/PhysRevLett.76.1804.
[23] Deza J, Barreiro M, Masoller C. Inferring interdependencies in climate networks constructed at inter-annual, intra-season and longer time scales. Eur Phys J Spec. Top 2013;222:511–23. http://dx.doi.org/10.1140/epjst/e2013-01856-5.
[24] Minati L, Chiesa P, Tabarelli D, D'Incerti L, Jovicich J. Synchronization, non-linear dynamics and low-frequency fluctuations: Analogy between spontaneous brain activity and networked single-transistor chaotic oscillators. Chaos 2015;25:033107. http://dx.doi.org/10.1063/1.4914938.
[25] Tirabassi G, Sevilla-Escoboza R, Buldú J, Masoller C. Inferring the connectivity of coupled oscillators from time-series statistical similarity analysis. Sci Rep 2015;5:10829. http://dx.doi.org/10.1038/srep10829.
[26] Burridge R, Knopoff L. Model and theoretical seismicity. Bull Seismol Soc Am 1967;57:341–71. http://dx.doi.org/10.1785/BSSA0570030341.
[27] Field S, Venturi N, Nori F. Marginal stability and chaos in coupled faults modeled by nonlinear circuits. Phys Rev Lett 1995;74:74–7. http://dx.doi.org/10.1103/PhysRevLett.74.74.
[28] Perinelli A, Iuppa R, Ricci L. A scalable electronic analog of the Burridge–Knopoff model of earthquake faults. Chaos 2023;33:093103. http://dx.doi.org/10.1063/5.0161339.
[29] Bandt C, Pompe B. Permutation entropy: A natural complexity measure for time series. Phys Rev Lett 2002;88(17):174102. http://dx.doi.org/10.1103/PhysRevLett.88.174102.
[30] Bahraminasab A, Ghasemi F, Stefanovska A, McClintock PVE, Kantz H. Direction of coupling from phases of interacting oscillators: A permutation information approach. Phys Rev Lett 2008;100:084101. http://dx.doi.org/10.1103/PhysRevLett.100.084101.
[31] Salvador R, Suckling J, Coleman MR, Pickard JD, Menon D, Bullmore E. Neurophysiological architecture of functional magnetic resonance images of human brain. Cereb Cortex 2005;15:1332–42. http://dx.doi.org/10.1093/cercor/bhi016.
[32] Salvador R, Suckling J, Schwarzbauer C, Bullmore E. Undirected graphs of frequency–dependent functional connectivity in whole brain networks. Philos Trans R Soc B 2005;360:937–46. http://dx.doi.org/10.1098/rstb.2005.1645.
[33] Fair DA, Cohen AL, Power JD, Dosenbach NUF, Church JA, Miezin FM, et al. Functional brain networks develop from a local to distributed organization. PLoS Comput Biol 2009;5:e1000381. http://dx.doi.org/10.1371/journal.pcbi.1000381.
[34] Perinelli A, Tabarelli D, Miniussi C, Ricci L. Dependence of connectivity on geometric distance in brain networks. Sci Rep 2019;9:13412. http://dx.doi.org/10.1038/s41598-019-50106-2.
[35] Minati L, Ito H, Perinelli A, Ricci L, Faes L, Yoshimura N, et al. Connectivity influences on nonlinear dynamics in weakly-synchronized networks: Insights from rössler systems, electronic chaotic oscillators, model and biological neurons. IEEE Access 2019;7:174793–821. http://dx.doi.org/10.1109/ACCESS.2019.2957014.
[36] Ricci L, Perinelli A, Castelluzzo M, Euzzor S, Meucci R. Experimental evidence of chaos generated by a minimal universal oscillator model. Int J Bifurcat Chaos 2021;31:2150205. http://dx.doi.org/10.1142/S0218127421502059.
[37] Missiaggia M, Pierobon E, Castelluzzo M, Perinelli A, Cordoni F, Centis Vignali M, et al. A novel hybrid microdosimeter for radiation field characterization based on the tissue equivalent proportional counter detector and low gain avalanche detectors tracker: A feasibility study. Front Phys 2021;8:578444. http://dx.doi.org/10.3389/fphy.2020.578444.
[38] Grün S. Data-driven significance estimation for precise spike correlation. J Neurophysiol 2009;101:1126–40. http://dx.doi.org/10.1152/jn.00093.2008.
[39] Ricci L, Castelluzzo M, Minati L, Perinelli A. Generation of surrogate event sequences via joint distribution of successive inter-event intervals. Chaos 2019;29:121102. http://dx.doi.org/10.1063/1.5138250.
[40] Granger CWJ. Investigating causal relations by econometric models and cross-spectral methods. Econometrica 1969;37:424–38. http://dx.doi.org/10.2307/1912791.
[41] Baccalá LA, Sameshima K. Partial directed coherence: a new concept in neural structure determination. Biol Cybernet 2001;84:463–74. http://dx.doi.org/10.1007/PL00007990.
[42] Kamiński M, Ding M, Truccolo WA, Bressler SL. Evaluating causal relations in neural systems: Granger causality, directed transfer function and statistical assessment of significance. Biol Cybernet 2001;85:145–57. http://dx.doi.org/10.1007/s004220000235.
[43] Chen Y, Rangarajan G, Feng J, Ding M. Analyzing multiple nonlinear time series with extended Granger causality. Phys Lett A 2004;324:26–35. http://dx.doi.org/10.1016/j.physleta.2004.02.032.
[44] Marinazzo D, Pellicoro M, Stramaglia S. Nonlinear parametric model for Granger causality of time series. Phys Rev E 2006;73:066216. http://dx.doi.org/10.1103/PhysRevE.73.066216.
[45] Rosenblum MG, Pikovsky AS. Detecting direction of coupling in interacting oscillators. Phys Rev E 2001;64:045202. http://dx.doi.org/10.1103/PhysRevE.64.045202.
[46] Paluš M, Stefanovska A. Direction of coupling from phases of interacting oscillators: An information-theoretic approach. Phys Rev E 2003;67:055201. http://dx.doi.org/10.1103/PhysRevE.67.055201.
[47] Faes L, Porta A, Nollo G. Information-based detection of nonlinear Granger causality in multivariate processes via a nonuniform embedding technique. Phys Rev E 2011;83:051112. http://dx.doi.org/10.1103/PhysRevE.83.051112.
[48] Silini R, Tirabassi G, Barreiro M, Ferranti L, Masoller C. Assessing causal dependencies in climatic indices. Clim Dyn 2023;61:79–89. http://dx.doi.org/10.1007/s00382-022-06562-0.
[49] Timme M. Revealing network connectivity from response dynamics. Phys Rev Lett 2007;98:224101. http://dx.doi.org/10.1103/PhysRevLett.98.224101.